International Journal of Heat and Mass Transfer 51 (2008) 5380–5388

Contents lists available at ScienceDirect

International Journal of Heat and Mass Transfer

journal homepage: www.elsevier.com/locate/ijhmt

A regularized integral equation method for the inverse geometry heat conduction problem

Chein-Shan Liu [a,b,*], Chih-Wen Chang [c], Chia-Yen Chiang [c]

[a] Department of Mechanical and Mechatronic Engineering, National Taiwan Ocean University, Keelung 20224, Taiwan
[b] Department of Harbor and River Engineering, National Taiwan Ocean University, Keelung 20224, Taiwan
[c] Department of Systems Engineering and Naval Architecture, National Taiwan Ocean University, Keelung 20224, Taiwan

ARTICLE INFO

Article history:
Received 7 May 2007
Received in revised form 24 January 2008
Available online 20 May 2008

Keywords:
Inverse geometry heat conduction problem
Fredholm integral equation
Two-point boundary value problem
Collocation method
Lavrentiev regularization
Fourier series
Regularized solution

ABSTRACT

This paper addresses a new technique for solving the inverse geometry heat conduction problem of the Laplace equation in a two-dimensional rectangle, which, named regularized integral equation method (RIEM), consists of three parts. First of all, the Fourier series expansion technique is used to calculate the temperature field $u(x,y)$. Second, we consider a Lavrentiev regularization by adding a term $\alpha g(x)$ to obtain a second kind Fredholm integral equation. The termwise separable property of the kernel function allows us to transform the inverse geometry heat conduction problem into a two-point boundary value problem and therefore, an analytical regularized solution is derived in the final part by using orthogonality. Principally, the RIEM possesses the following advantages: it does not need any guess of the initial profile, it does not need any iteration and a regularized closed-form solution can be obtained. The uniform convergence and error estimate of the regularized solution $u^{\alpha}(x,y)$ are proved and a boundary geometry $p(x)$ is solved by half-interval method. Several numerical examples present the effectiveness of our novel approach in providing excellent estimates of unknown boundary shapes from given data.

© 2008 Elsevier Ltd. All rights reserved.

1. Introduction

Over the last several decades, much interest has been directed towards the use of inverse techniques for solving different engineering problems that cannot be described mathematically by direct approaches. This situation arises when all the required data to cope with a direct problem or to attain a reliable direct solution are not available. The inverse problem can be defined as a problem that one or more conditions are absent for a corresponding direct problem. Such a problem is much more difficult to solve than a direct one.

The inverse geometry heat conduction problem is ill-posed in the sense that from the external measurements on one side we have an incomplete data set from which we are required to identify unknown irregular boundary configurations. In order to solve the problem, the progresses have been made, including the Levenberg–Marquardt method [5], the conjugate gradient method [1–9], the simplified conjugate gradient method [10], and the steepest descent method [11]. Recently, many researchers have concentrated on infrared scanners and their applications to nondestructive evaluation [12–14].

In the present paper, we cast the inverse geometry heat conduction problem into a first kind Fredholm integral equation, and then we address a Lavrentiev regularization to transform it into a second kind Fredholm integral equation. By employing the kernel function separate characteristic and eigenfunctions expansion technique, we can derive an analytical solution of the second kind Fredholm integral equation. This method was first used by Liu [15] to solve a direct problem of elastic torsion in an arbitrary plane domain, where it was called a meshless regularized integral equation method. Then, Liu [16,17] extended it to solve the Laplace direct problem in arbitrary plane domains. The novel method employs a laconic numerical implementation to cope with the difficulties of the inverse geometry heat conduction problem.

2. The collocation method

We consider a two-dimensional steady-state heat conduction problem given as follows:

$$u_{xx} + u_{yy} = 0, \quad 0 < x < \ell, \tag{1}$$
$$u_x(0,y) = u_x(\ell,y) = 0, \tag{2}$$
$$u(x,0) = f(x), \quad 0 \leqslant x \leqslant \ell, \tag{3}$$
$$u_y(x,0) = -q_0, \quad 0 \leqslant x \leqslant \ell, \tag{4}$$
$$u(x,p(x)) = u_0, \quad 0 \leqslant x \leqslant \ell, \tag{5}$$

* Corresponding author. Address: Department of Mechanical and Mechatronic Engineering, National Taiwan Ocean University, Keelung 20224, Taiwan. Tel.: +886 2 24622192x3252; fax: +886 2 24620836.
E-mail address: csliu@mail.ntou.edu.tw (C.-S. Liu).

0017-9310/$ - see front matter © 2008 Elsevier Ltd. All rights reserved.
doi:10.1016/j.ijheatmasstransfer.2008.02.043

Nomenclature

a_0	Fourier coefficient defined in Eq. (21)
a_k	Fourier coefficient defined in Eq. (22)
A_0	Fourier coefficient defined in Eq. (7)
A_k	Fourier coefficient defined in Eq. (8)
$\mathbf{A}$	a matrix defined in Eq. (16)
b	y-axial length
$\mathbf{b}$	a vector defined in Eq. (16)
b_0	Fourier coefficient defined in Eq. (23)
b_k	Fourier coefficient defined in Eq. (24)
b_0^*	Fourier coefficient defined in Eq. (58)
b_k^*	Fourier coefficient defined in Eq. (59)
$\mathbf{c}$	a constant vector used in Eq. (14)
c_{k+1}	a constant used in Eq. (18)
$\mathbf{d}$	a constant vector used in Eq. (42)
e_0	a constant defined in Eq. (66)
e_k	a constant defined in Eq. (67)
$f(x)$	a given function maybe obtained through measurement
$g(x)$	an unknown function
$\mathbf{I}_{m+1}$	$m+1$-dimensional unit matrix
$K(x,\xi)$	the Kernel defined in Eq. (29)
ℓ	x-axial length
$L^2(0,\ell)$	set of square-integrable functions on $(0,\ell)$
m	the summation upper bound used in Eqs. (10) and (31)
M	a sequence of positive numbers
$p(x)$	an unknown boundary geometry
q_0	a constant heat flux
$\mathbf{P}$, $\mathbf{Q}$	m-vectors defined in Eq. (33)
$R(i)$	random numbers
$\mathbf{R}$	a matrix defined in Eq. (47)
u	temperature distribution
u_0	a constant temperature
u^α	regularized solution
$\mathbf{u}_1(x)$	vector-valued function of x defined in Eq. (35)
$\mathbf{u}_2(x)$	vector-valued function of x defined in Eq. (36)
x	space variable

Greek symbols

α	regularized parameter
δ_{jk}	the Kronecker delta
ε	belongs to $(0,1)$
ξ	space variable used in Eq. (7)
σ	noise level

Subscripts and superscripts

i	index
jk	indices
k	index
T	transpose

where $f(x)$ is a given function perhaps obtained through measurement, q_0 is a given constant heat flux, u_0 is a given constant temperature, and $p(x)$ is an unknown boundary geometry to be determined under an overspecified data of $f(x)$. The problem setup with its physical model, the geometry and the coordinates are shown in Fig. 1.

The present inverse problem is to use the data u_0, q_0 and $f(x)$ to find the unknown shape function $p(x)$, where the temperature is fixed to be u_0. Here, we tentatively assume that $p(x)$ is a known function in order to compare it with our numerical result of the boundary shape function $p(x)$ reconstructed by the present new method and assess the accuracy of the new method.

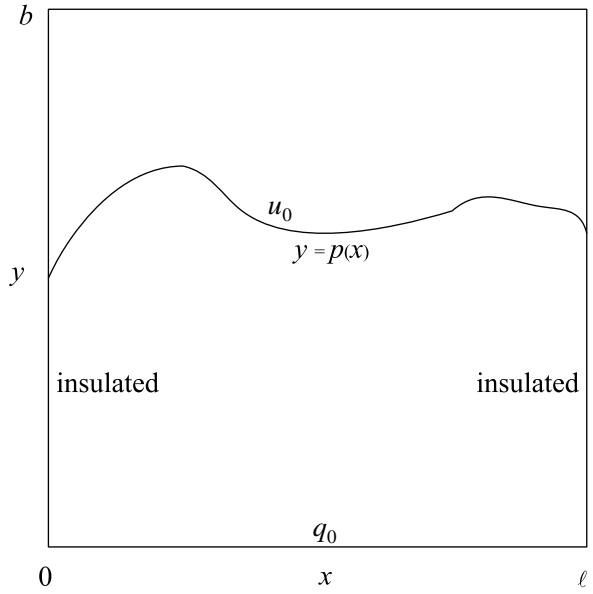

Fig. 1. Shape geometry and x–y coordinates.

For the given constants q_0 and u_0 and the given function $p(x)$, there were many numerical approaches which could be employed to solve the direct problem for giving the data of $f(x)$. We will use the collocation method to calculate the data $f(x)$ if it is not available. In [5], the function $f(x)$ is obtained from the measured temperature data at the bottom of a rectangle.

However, in order to obtain the function $f(x)$ for the later use we address a different numerical method. Suppose that $g(x)$ is an unknown function with $u(x,b) = g(x)$, where b is a constant determined by the user, only requiring $b > p(x)$, which together with conditions (2) and (4) lead to

$$u(x,y) = A_0 - q_0(y-b) + \sum_{k=1}^{\infty} A_k \frac{\cosh(k\pi y/\ell)}{\sinh(bk\pi/\ell)} \cos\frac{k\pi x}{\ell}, \tag{6}$$

where

$$A_0 = \frac{1}{\ell}\int_0^{\ell} g(\xi)\mathrm{d}\xi, \tag{7}$$

$$A_k = \frac{2\tanh(bk\pi/\ell)}{\ell}\int_0^{\ell} g(\xi)\cos\frac{k\pi\xi}{\ell}\,\mathrm{d}\xi. \tag{8}$$

We are going to employ the collocation method to determine the unknown coefficients when the boundary geometry $p(x)$ is given.

By imposing condition (5) on Eq. (6), we obtain

$$A_0 + \sum_{k=1}^{\infty}\left\{A_k\frac{\cosh(k\pi p(x)/\ell)}{\sinh(bk\pi/\ell)}\right\}\cos\frac{k\pi x}{\ell} = u_0 + q_0 p(x) - q_0 b. \tag{9}$$

Eq. (9) can be used to determine the unknown coefficients in Eq. (6).

The series expansion in Eq. (9) is well suited in the range of $x \in [0,\ell]$. Therefore, we may have an admissible function with finite terms

$$A_0 + \sum_{k=1}^{m}\left\{A_k\frac{\cosh(k\pi p(x)/\ell)}{\sinh(bk\pi/\ell)}\right\}\cos\frac{k\pi x}{\ell} = u_0 + q_0 p(x) - q_0 b,\quad 0 \leqslant x \leqslant \ell. \tag{10}$$

Our task below is to find A_k, $k = 0,1,\ldots,m$ from Eq. (10).

Eq. (10) is imposed at $n = m + 1$ different collocated points x_i on the interval with $0 \leqslant x_i \leqslant \ell$:

$$A_0 + \sum_{k=1}^{m} \left\{ A_k \frac{\cosh(k\pi p(x_i)/\ell)}{\sinh(bk\pi/\ell)} \right\} \cos\frac{k\pi x_i}{\ell} = u_0 + q_0 p(x_i) - q_0 b. \tag{11}$$

Let

$$x_i = i\Delta x, \quad i = 0, 1, \ldots, m, \tag{12}$$

where $\Delta x = \ell/n$. When the index i in Eq. (11) runs from 0 to m, we obtain a linear equations system with dimensions $n = m + 1$:

$$\begin{bmatrix} 1 & \frac{\cosh[p(x_0)\pi/\ell]\cos(\pi x_0/\ell)}{\sinh(b\pi/\ell)} & \frac{\cosh[2p(x_0)\pi/\ell]\cos(2\pi x_0/\ell)}{\sinh(2b\pi/\ell)} & \cdots & \frac{\cosh[mp(x_0)\pi/\ell]\cos(m\pi x_0/\ell)}{\sinh(mb\pi/\ell)} \\ 1 & \frac{\cosh[p(x_1)\pi/\ell]\cos(\pi x_1/\ell)}{\sinh(b\pi/\ell)} & \frac{\cosh[2p(x_1)\pi/\ell]\cos(2\pi x_1/\ell)}{\sinh(2b\pi/\ell)} & \cdots & \frac{\cosh[mp(x_1)\pi/\ell]\cos(m\pi x_1/\ell)}{\sinh(mb\pi/\ell)} \\ 1 & \frac{\cosh[p(x_2)\pi/\ell]\cos(\pi x_2/\ell)}{\sinh(b\pi/\ell)} & \frac{\cosh[2p(x_2)\pi/\ell]\cos(2\pi x_2/\ell)}{\sinh(2b\pi/\ell)} & \cdots & \frac{\cosh[mp(x_2)\pi/\ell]\cos(m\pi x_2/\ell)}{\sinh(mb\pi/\ell)} \\ \vdots & \vdots & \vdots & \vdots & \vdots \\ 1 & \frac{\cosh[p(x_{m-1})\pi/\ell]\cos(\pi x_{m-1}/\ell)}{\sinh(b\pi/\ell)} & \frac{\cosh[2p(x_{m-1})\pi/\ell]\cos(2\pi x_{m-1}/\ell)}{\sinh(2b\pi/\ell)} & \cdots & \frac{\cosh[mp(x_{m-1})\pi/\ell]\cos(m\pi x_{m-1}/\ell)}{\sinh(mb\pi/\ell)} \\ 1 & \frac{\cosh[p(x_m)\pi/\ell]\cos(\pi x_m/\ell)}{\sinh(b\pi/\ell)} & \frac{\cosh[2p(x_m)\pi/\ell]\cos(2\pi x_m/\ell)}{\sinh(2b\pi/\ell)} & \cdots & \frac{\cosh[mp(x_m)\pi/\ell]\cos(m\pi x_m/\ell)}{\sinh(mb\pi/\ell)} \end{bmatrix} \begin{bmatrix} A_0 \\ A_1 \\ A_2 \\ \vdots \\ A_m \end{bmatrix} = \begin{bmatrix} u_0 + q_0[p(x_0) - b] \\ u_0 + q_0[p(x_1) - b] \\ u_0 + q_0[p(x_2) - b] \\ \vdots \\ u_0 + q_0[p(x_{m-1}) - b] \\ u_0 + q_0[p(x_m) - b] \end{bmatrix}. \tag{13}$$

We denote the above equation by

$$\mathbf{Rc} = \mathbf{h}, \tag{14}$$

where $\mathbf{c} = (c_1, \ldots, c_{m+1})^{\mathrm{T}} = (A_0, A_1, A_2, \ldots, A_m)^{\mathrm{T}}$ is the vector of unknown coefficients. The superscript T represents the transpose.

The conjugate gradient method can be used to solve the following normal equation with a specified convergent criterion, e.g., $\varepsilon = 10^{-6}$:

$$\mathbf{Ac} = \mathbf{b}, \tag{15}$$

where

$$\mathbf{A} := \mathbf{R}^{\mathrm{T}}\mathbf{R}, \mathbf{b} := \mathbf{R}^{\mathrm{T}}\mathbf{h}. \tag{16}$$

Inserting the calculated $\mathbf{c}$ into Eq. (6), we can calculate $u(x,y)$ at any point in the problem domain by

$$u(x,y) = c_1 - q_0(y - b) + \sum_{k=1}^{m} \left[c_{k+1} \frac{\cosh(k\pi y/\ell)}{\sinh(bk\pi/\ell)} \right] \cos\frac{k\pi x}{\ell}. \tag{17}$$

Therefore, in view of Eq. (3) by inserting $y = 0$ into the above equation we can obtain the following data:

$$f(x) = c_1 + q_0 b + \sum_{k=1}^{m} \left[\frac{c_{k+1}}{\sinh(bk\pi/\ell)} \right] \cos\frac{k\pi x}{\ell}. \tag{18}$$

3. The inverse geometry heat conduction problem

The present inverse geometry heat conduction problem is to determine the boundary shape $p(x)$ in Eq. (5) by using the over-specified boundary conditions (3) and (4) on the bottom side.

In order to solve the inverse geometry heat conduction problem, we assume that there exists an unknown function $g(x) \in L^2(0,\ell)$ such that $u(x,b) = g(x)$. Thus, in place of Eq. (4) we consider the following boundary condition:

$$u(x,b) = g(x), \quad 0 \leqslant x \leqslant \ell, \tag{19}$$

where $g(x)$ is an unknown function to be determined below.

By utilizing the technique of separation of variables, we are apt to write a series expansion of $u(x,y)$ satisfying Eqs. (1)–(3) and (19):

$$u(x,y) = a_0(b - y) + b_0 y + \sum_{k=1}^{\infty} \left\{ a_k \frac{\sinh[(b-y)k\pi/\ell]}{\sinh(bk\pi/\ell)} + b_k \frac{\sinh(k\pi y/\ell)}{\sinh(bk\pi/\ell)} \right\} \cos\frac{k\pi x}{\ell}, \tag{20}$$

where

$$a_0 = \frac{1}{b\ell} \int_0^{\ell} f(\xi)\mathrm{d}\xi, \tag{21}$$

$$a_k = \frac{2}{\ell} \int_0^{\ell} f(\xi) \cos\frac{k\pi\xi}{\ell}\mathrm{d}\xi, \tag{22}$$

$$b_0 = \frac{1}{b\ell} \int_0^{\ell} g(\xi)\mathrm{d}\xi, \tag{23}$$

$$b_k = \frac{2}{\ell} \int_0^{\ell} g(\xi) \cos\frac{k\pi\xi}{\ell}\mathrm{d}\xi. \tag{24}$$

If $g(x)$ is available, which together with the given or measured $f(x)$ we can calculate all the above coefficients, and then using Eq. (20) to solve $p(x)$ from $u(x,p(x)) = u_0$ by the half-interval method, we can attain a boundary geometry along which the temperature is u_0.

4. The Fredholm integral equation

In the following three sections, we will derive a new method to find the unknown function $g(x)$. Taking the differential of Eq. (20) with respect to y, we obtain

$$\frac{\partial u(x,y)}{\partial y} = b_0 - a_0 + \sum_{k=1}^{\infty} \frac{k\pi}{\ell} \left\{ -a_k \frac{\cosh[(b-y)k\pi/\ell]}{\sinh(bk\pi/\ell)} + b_k \frac{\cosh(k\pi y/\ell)}{\sinh(bk\pi/\ell)} \right\} \cos\frac{k\pi x}{\ell}. \tag{25}$$

By imposing the condition in Eq. (4) on the above equation, we attain

$$b_0 + \frac{\pi}{\ell} \sum_{k=1}^{\infty} b_k \frac{k}{\sinh(bk\pi/\ell)} \cos\frac{k\pi x}{\ell} = h(x), \tag{26}$$

where

$$h(x) = a_0 + \frac{\pi}{\ell} \sum_{k=1}^{\infty} a_k \frac{k\cosh(bk\pi/\ell)}{\sinh(bk\pi/\ell)} \cos\frac{k\pi x}{\ell} - q_0. \tag{27}$$

Substituting Eq. (23) for b_0 and Eq. (24) for b_k into Eq. (26), it follows that

$$\int_0^{\ell} K(x,\xi) g(\xi)\mathrm{d}\xi = h(x), \tag{28}$$

where

$$K(x,\xi) = \frac{1}{b\ell} + \frac{2\pi}{\ell^2} \sum_{k=1}^{\infty} \frac{k}{\sinh(bk\pi/\ell)} \cos\frac{k\pi x}{\ell} \cos\frac{k\pi\xi}{\ell} \tag{29}$$

is a kernel function.

In order to obtain $g(x)$, we have to deal with the first kind Fredholm integral Eq. (28), which is known to be ill-posed.

5. Two-point boundary value problem

We suppose that there exists a regularized parameter α, such that Eq. (28) can be regularized by

$$\alpha g(x)+\int_0^\ell K(x,\xi)g(\xi)\mathrm{d}\xi=h(x), \tag{30}$$

which is a second kind Fredholm integral equation. This regularization technique is known as the Lavrentiev regularization [18]. We also presume that the kernel function can be approximated by m terms with

$$K(x,\xi)=\frac{1}{b\ell}+\frac{2\pi}{\ell^2}\sum_{k=1}^{m}\frac{k}{\sinh(bk\pi/\ell)}\cos\frac{k\pi x}{\ell}\cos\frac{k\pi\xi}{\ell}. \tag{31}$$

However, this supposition is not essential, because when the required equations are derived, we can supersede m by ∞ again. It can be seen below that Eq. (30) is well-posed and the above series is convergent.

By inspection, we have

$$K(x,\xi)=\mathbf{P}(x)\cdot\mathbf{Q}(\xi), \tag{32}$$

where $\mathbf{P}$ and $\mathbf{Q}$ are m-vectors given by

$$\mathbf{P}:=\begin{bmatrix}\frac{1}{b\ell}\\ \frac{2\pi}{\ell^2\sinh(b\pi/\ell)}\cos\frac{\pi x}{\ell}\\ \frac{4\pi}{\ell^2\sinh(2b\pi/\ell)}\cos\frac{2\pi x}{\ell}\\ \vdots\\ \frac{2m\pi}{\ell^2\sinh(\mathrm{mb}\pi/\ell)}\cos\frac{m\pi x}{\ell}\end{bmatrix},\quad \mathbf{Q}:=\begin{bmatrix}1\\ \cos\frac{\pi\xi}{\ell}\\ \cos\frac{2\pi\xi}{\ell}\\ \vdots\\ \cos\frac{m\pi\xi}{\ell}\end{bmatrix} \tag{33}$$

and the dot between $\mathbf{P}$ and $\mathbf{Q}$ denotes the inner product, which is sometime written as $\mathbf{P}^{\mathrm{T}}\mathbf{Q}$ for convenience. With the aid of Eq. (32), Eq. (30) can be decomposed as

$$\alpha g(x)+\int_0^x\mathbf{P}^{\mathrm{T}}(x)\mathbf{Q}(\xi)g(\xi)\mathrm{d}\xi+\int_x^\ell\mathbf{P}^{\mathrm{T}}(x)\mathbf{Q}(\xi)g(\xi)\mathrm{d}\xi=h(x). \tag{34}$$

Let us define

$$\mathbf{u}_1(x):=\int_0^x\mathbf{Q}(\xi)g(\xi)\mathrm{d}\xi, \tag{35}$$

$$\mathbf{u}_2(x):=\int_\ell^x\mathbf{Q}(\xi)g(\xi)\mathrm{d}\xi \tag{36}$$

and Eq. (34) can be expressed as

$$\alpha g(x)+\mathbf{P}^{\mathrm{T}}(x)[\mathbf{u}_1(x)-\mathbf{u}_2(x)]=h(x). \tag{37}$$

Taking the differentials of Eqs. (35) and (36) with respect to x, we obtain

$$\mathbf{u}_1'(x)=\mathbf{Q}(x)g(x), \tag{38}$$

$$\mathbf{u}_2'(x)=\mathbf{Q}(x)g(x). \tag{39}$$

Inserting Eq. (37) for $g(x)$ into the above two equations, we acquire

$$\alpha\mathbf{u}_1'(x)=\mathbf{Q}(x)\mathbf{P}^{\mathrm{T}}(x)[\mathbf{u}_2(x)-\mathbf{u}_1(x)]+h(x)\mathbf{Q}(x),\quad \mathbf{u}_1(0)=\mathbf{0}, \tag{40}$$

$$\alpha\mathbf{u}_2'(x)=\mathbf{Q}(x)\mathbf{P}^{\mathrm{T}}(x)[\mathbf{u}_2(x)-\mathbf{u}_1(x)]+h(x)\mathbf{Q}(x),\quad \mathbf{u}_2(\ell)=\mathbf{0}, \tag{41}$$

where the last two conditions follow from Eqs. (35) and (36) readily. The above two equations constitute a two-point boundary value problem.

6. An analytical regularized solution

In this section, we will find an analytical solution for $g(x)$. From Eqs. (38) and (39), it can be seen that $\mathbf{u}_1'=\mathbf{u}_2'$, which means that

$$\mathbf{u}_1=\mathbf{u}_2+\mathbf{d}, \tag{42}$$

where $\mathbf{d}$ is a constant vector to be determined. By using the final condition in Eq. (41), we find that

$$\mathbf{u}_1(\ell)=\mathbf{u}_2(\ell)+\mathbf{d}=\mathbf{d}. \tag{43}$$

Substituting Eq. (42) into (40), we have

$$\alpha\mathbf{u}_1'(x)=-\mathbf{Q}(x)\mathbf{P}^{\mathrm{T}}(x)\mathbf{d}+h(x)\mathbf{Q}(x),\quad \mathbf{u}_1(0)=\mathbf{0}. \tag{44}$$

Integrating and using the initial condition, it follows that

$$\mathbf{u}_1(x)=\frac{-1}{\alpha}\int_0^x\mathbf{Q}(\xi)P^{\mathrm{T}}(\xi)\mathrm{d}\xi\mathbf{d}+\frac{1}{\alpha}\int_0^x h(\xi)\mathbf{Q}(\xi)\mathrm{d}\xi. \tag{45}$$

Taking $x=\ell$ in the above equation and imposing the condition (43), one obtains a governing equation for $\mathbf{d}$:

$$\mathbf{R}\mathbf{d}=\int_0^\ell h(\xi)\mathbf{Q}(\xi)\mathrm{d}\xi, \tag{46}$$

where

$$\mathbf{R}:=\alpha\mathbf{I}_{m+1}+\int_0^\ell\mathbf{Q}(\xi)\mathbf{P}^{\mathrm{T}}(\xi)\mathrm{d}\xi. \tag{47}$$

It is straightforward to write

$$\mathbf{d}=\mathbf{R}^{-1}\int_0^\ell h(\xi)\mathbf{Q}(\xi)\mathrm{d}\xi. \tag{48}$$

On the other hand, from Eqs. (37) and (42) we have

$$\alpha g(x)=h(x)-\mathbf{P}(x)\cdot\mathbf{d}. \tag{49}$$

Inserting Eq. (48) into the above equation, we obtain

$$\alpha g(x)=h(x)-\mathbf{P}(x)\cdot\mathbf{R}^{-1}\int_0^\ell h(\xi)\mathbf{Q}(\xi)\mathrm{d}\xi. \tag{50}$$

Due to the orthogonality of

$$\int_0^\ell\cos\frac{j\pi\xi}{\ell}\cos\frac{k\pi\xi}{\ell}\mathrm{d}\xi=\frac{\ell}{2}\delta_{jk}, \tag{51}$$

where δ_{jk} is the Kronecker delta, the $(m+1)\times(m+1)$ matrix can be written as

$$\int_0^\ell\mathbf{Q}(\xi)\mathbf{P}^{\mathrm{T}}(\xi)\mathrm{d}\xi=\mathrm{diag}\left[\frac{1}{b},\frac{\pi}{\ell\sinh(b\pi/\ell)},\frac{2\pi}{\ell\sinh(2b\pi/\ell)},\ldots,\frac{m\pi}{\ell\sinh(mb\pi/\ell)}\right], \tag{52}$$

where diag means that the matrix is a diagonal matrix. Inserting Eq. (52) into Eq. (50), we therefore obtain

$$g(x)=\frac{1}{\alpha}h(x)-\frac{1}{\alpha}\mathbf{P}^{\mathrm{T}}(x)\mathrm{diag}\left[\frac{b}{1+b\alpha},\frac{1}{\alpha+\frac{\pi}{\ell\sinh(b\pi/\ell)}},\frac{1}{\alpha+\frac{2\pi}{\ell\sinh(2b\pi/\ell)}},\ldots,\frac{1}{\alpha+\frac{m\pi}{\ell\sinh(mb\pi/\ell)}}\right]\int_0^\ell h(\xi)\mathbf{Q}(\xi)\mathrm{d}\xi. \tag{53}$$

While we use Eq. (33) for $\mathbf{P}$ and $\mathbf{Q}$, we can get

$$g(x)=\frac{1}{\alpha}h(x)-\frac{1}{\alpha\ell(1+b\alpha)}\int_0^\ell h(\xi)\mathrm{d}\xi-\frac{2}{\alpha\ell}\sum_{k=1}^{\infty}\frac{\frac{k\pi}{\ell\sinh(kb\pi/\ell)}}{\alpha+\frac{k\pi}{\ell\sinh(kb\pi/\ell)}}\times\int_0^\ell\cos\frac{k\pi x}{\ell}\cos\frac{k\pi\xi}{\ell}h(\xi)\mathrm{d}\xi. \tag{54}$$

Because our argument to derive the above equation does not depend on m, we have replaced $m\psi$ by ∞. For a given $h(x)$ by Eq. (27), we may employ the above equation to calculate $g(x)$.

Moreover, if $g(x)$ in Eq. (54) is available, we can insert it into Eqs. (23) and (24) and utilize the orthogonality Eq. (51) to acquire

$$b_0=\frac{1}{\ell(1+b\alpha)}\int_0^\ell h(\xi)\mathrm{d}\xi, \tag{55}$$

$$b_k=\frac{2}{\ell\left[\alpha+\frac{k\pi}{\ell\sinh(kb\pi/\ell)}\right]}\int_0^\ell\cos\frac{k\pi\xi}{\ell}h(\xi)\mathrm{d}\xi. \tag{56}$$

Then, from Eq. (20) we can calculate $u^{\alpha}(x,y)$, where we use the symbol $u^{\alpha}(x,y)$ to denote the present solution is a regularized one. Fig. 2 displays the flow chart of RIEM.

7. Error estimation

In the previous section, we have derived a regularized solution $u^\alpha(x,y)$ of Eqs. (1)–(4) under the regularized format (30) with a regularized parameter $\alpha > 0$. We can prove the following main results.

Taking $\alpha = 0$ in Eqs. (55) and (56) and inserting them into Eq. (20), we obtain a formal solution of Eqs. (1)–(4):

$$u(x,y) = a_0(b-y) + b_0^* y + \sum_{k=1}^{\infty}\left\{a_k\frac{\sinh[(b-y)k\pi/\ell]}{\sinh(bk\pi/\ell)} + b_k^*\frac{\sinh(k\pi y/\ell)}{\sinh(bk\pi/\ell)}\right\}\cos\frac{k\pi x}{\ell}, \tag{57}$$

where a_0 and a_k are still given by Eqs. (21) and (22) and

$$b_0^* = \frac{1}{\ell}\int_0^\ell h(\xi)\mathrm{d}\xi, \tag{58}$$

$$b_k^* = \frac{2}{\frac{k\pi}{\sinh(kb\pi/\ell)}}\int_0^\ell \cos\frac{k\pi\xi}{\ell}h(\xi)\mathrm{d}\xi. \tag{59}$$

According to the above equations, we can prove the following results.

Theorem 1. *Suppose that the data $h(x) \in L^2(0,\ell)$. Then, the sufficient and necessary condition that the inverse problem (1)–(4) has a solution is that*

$$\frac{b^2}{4\ell^2}\left(\int_0^\ell h(\xi)\mathrm{d}\xi\right)^2 + \sum_{k=1}^{\infty}\frac{\sinh^2(kb\pi/\ell)}{k^2\pi^2}\left(\int_0^\ell \cos\frac{k\pi\xi}{\ell}h(\xi)\mathrm{d}\xi\right)^2 < \infty. \tag{60}$$

Proof. Inserting $y = b$ into Eq. (57) and noting Eqs. (19), (58) and (59), we have

$$g(x) = u(x,b) = \frac{b}{\ell}\int_0^\ell h(\xi)\mathrm{d}\xi + \sum_{k=1}^{\infty}\frac{2}{\frac{k\pi}{\sinh(kb\pi/\ell)}}\int_0^\ell \cos\frac{k\pi\xi}{\ell}h(\xi)\mathrm{d}\xi\cos\frac{k\pi x}{\ell}, \tag{61}$$

where $g(x) \in L^2(0,\ell)$. The above is a Fourier cosine series of $g(x)$, and by the Parseval equality we have

$$\frac{b^2}{\ell^2}\left(\int_0^\ell h(\xi)\mathrm{d}\xi\right)^2 + \sum_{k=1}^{\infty}\frac{4}{\left(\frac{k\pi}{\sinh(kb\pi/\ell)}\right)^2}\left(\int_0^\ell \cos\frac{k\pi\xi}{\ell}h(\xi)\mathrm{d}\xi\right)^2 = \|g(x)\|^2_{L^2(0,\ell)} < \infty. \tag{62}$$

This proves the sufficient and necessary condition. □

Theorem 2. *If the data $h(x)$ satisfies condition (60) and there exists an $\varepsilon \in (0,1)$, such that*

$$\frac{b^{2(1+\varepsilon)}}{2\ell^2}\left(\int_0^\ell h(\xi)\mathrm{d}\xi\right)^2 + \sum_{k=1}^{\infty}\left[\frac{\sinh^2(kb\pi/\ell)}{k^2\pi^2}\right]^{1+\varepsilon}\left(\int_0^\ell \cos\frac{k\pi\xi}{\ell}h(\xi)\mathrm{d}\xi\right)^2 := \frac{M^2(\varepsilon)}{2\ell} < \infty, \tag{63}$$

then for any $\alpha > 0$ the regularized solution $u^\alpha(x,t)$ satisfies the following error estimation:

$$\|u^\alpha(x,y) - u(x,y)\|_{L^2(0,\ell)} \leqslant \alpha^\varepsilon M(\varepsilon). \tag{64}$$

Proof. From Eqs. (20), (55)–(59) it follows that

$$u(x,y) - u^\alpha(x,y) = e_0 y + \sum_{k=1}^{\infty} e_k\frac{\sinh(k\pi y/\ell)}{\sinh(bk\pi/\ell)}\cos\frac{k\pi x}{\ell}, \tag{65}$$

where

$$e_0 = \frac{b\alpha}{\ell(1+b\alpha)}\int_0^\ell h(\xi)\mathrm{d}\xi, \tag{66}$$

$$e_k = \frac{2\alpha\sinh(kb\pi/\ell)}{k\pi\left[\alpha + \frac{k\pi}{\ell\sinh(kb\pi/\ell)}\right]}\int_0^\ell \cos\frac{k\pi\xi}{\ell}h(\xi)\mathrm{d}\xi. \tag{67}$$

Thus, for any $\varepsilon \in (0,1)$ we have the following estimation:

$$\begin{aligned}
&\|u(x,t) - u^\alpha(x,t)\|^2_{L^2(0,\ell)} \\
&\leqslant \frac{b^2\alpha^2}{\ell}[(b^{-1}+\alpha)^\varepsilon(b^{-1}+\alpha)^{1-\varepsilon}]^{-2}\left(\int_0^\ell h(\xi)\mathrm{d}\xi\right)^2 \\
&\quad + 2\ell\alpha^2\sum_{k=1}^{\infty}\left(\frac{\sinh(k\pi y/\ell)}{\sinh(bk\pi/\ell)}\right)^2\frac{\sinh^2(kb\pi/\ell)}{k^2\pi^2} \\
&\quad \times\left[\left(\alpha + \frac{k\pi}{\ell\sinh(kb\pi/\ell)}\right)^\varepsilon\left(\alpha + \frac{k\pi}{\ell\sinh(kb\pi/\ell)}\right)^{1-\varepsilon}\right]^{-2} \\
&\quad \times\left(\int_0^\ell \cos\frac{k\pi\xi}{\ell}h(\xi)\mathrm{d}\xi\right)^2 \\
&\leqslant \frac{b^2\alpha^2}{\ell}b^{2\varepsilon}\alpha^{-2+2\varepsilon}\left(\int_0^\ell h(\xi)\mathrm{d}\xi\right)^2 + 2\ell\alpha^2\sum_{k=1}^{\infty}\frac{\sinh^2(kb\pi/\ell)}{k^2\pi^2} \\
&\quad \times\left[\frac{\ell^2\sinh^2(kb\pi/\ell)}{k^2\pi^2}\right]^\varepsilon[\alpha^{1-\varepsilon}]^{-2}\left(\int_0^\ell \cos\frac{k\pi\xi}{\ell}h(\xi)\mathrm{d}\xi\right)^2 \\
&= \frac{\alpha^{2\varepsilon}}{\ell}b^{2(1+\varepsilon)}\left(\int_0^\ell h(\xi)\mathrm{d}\xi\right)^2 + 2\ell\alpha^{2\varepsilon}\sum_{k=1}^{\infty}\left[\frac{\sinh^2(kb\pi/\ell)}{k^2\pi^2}\right]^{1+\varepsilon} \\
&\quad \times\left(\int_0^\ell \cos\frac{k\pi\xi}{\ell}h(\xi)\mathrm{d}\xi\right)^2.
\end{aligned} \tag{68}$$

Therefore, we complete the proof. □

The above two theorems are vital to verify that the proposed regularization is workable. Although the problem we consider is ill-posed, we have assumed that the exact solution is existent in order to cast the error estimate in a manner that is typical in partial differential equation approximations.

8. Numerical examples

Before embarking the numerical study of the novel solver, we are interested in its stability, when the boundary measured data are contaminated by random noise. We can assess the stability by adding different level of random noise on the boundary measured data and investigate its effect. We employ the function RANDOM_NUMBER given in Fortran to generate the noisy data $R(i)$, where $R(i)$ are random numbers in (0, 1). Therefore, we use the Gaussian noise given by [19]

$$\hat{f}(x_i) = f(x_i) + \sigma\sqrt{-2\ln(RR)/RR}[2R(i)-1], \tag{69}$$

$$RR = R^2(i) + [2R(i)-1]^2. \tag{70}$$

8.1. Example 1

In the first example we consider the inverse geometry problem with $f(x)$ given exactly. Therefore, we can directly skip to Section 6 by using the RIEM to solve this problem.

When $u(x,b) = 100\cos(\pi x/\ell)$ is given, we can easily to write a solution of $u(x,y)$ satisfying Eqs. (1)–(4):

$$u(x,y) = a_0(b-y) + b_0 y + \left\{a_1\frac{\sinh[(b-y)\pi/\ell]}{\sinh(b\pi/\ell)} + b_1\frac{\sinh(\pi y/\ell)}{\sinh(b\pi/\ell)}\right\}\cos\frac{\pi x}{\ell}, \tag{71}$$

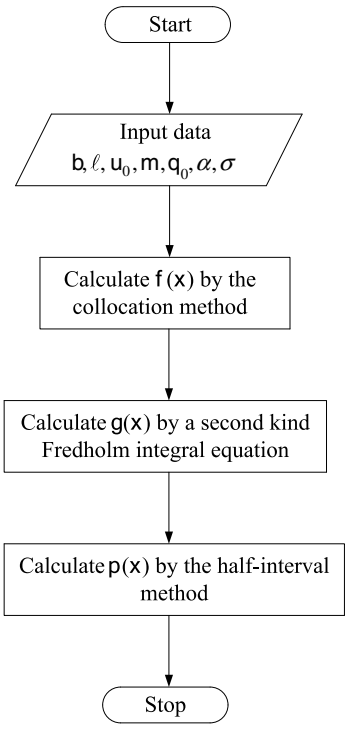

Fig. 2. Flow chart showing the process of the RIEM.

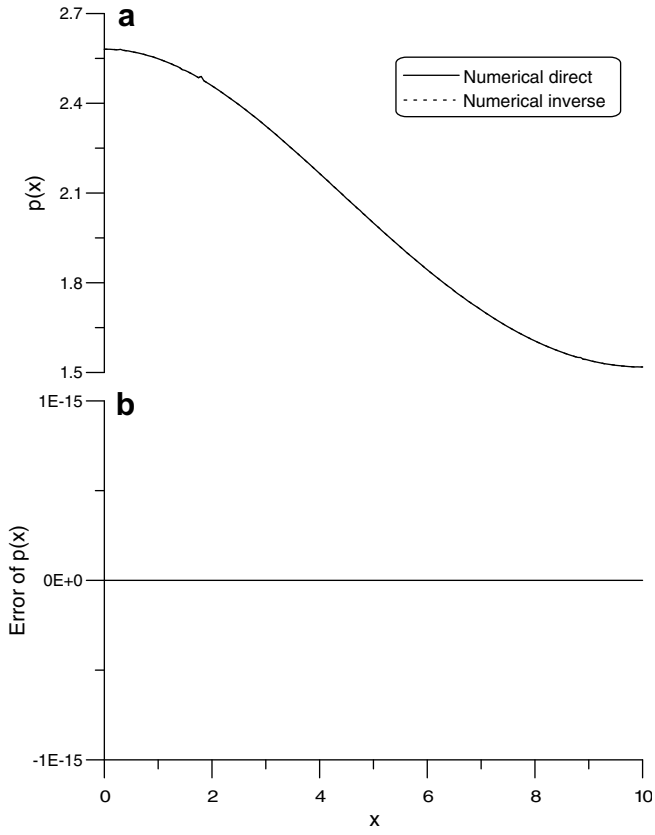

Fig. 3. For Example 1 we compare the boundary geometry obtained by the RIEM with the direct solution in (a), and the numerical error of $p(x)$ in (b).

where

$$a_0 = q_0, \tag{72}$$

$$a_1 = \frac{100}{\cosh(b\pi/\ell)}, \tag{73}$$

$$b_0 = 0, \tag{74}$$

$$b_1 = 100. \tag{75}$$

Substituting Eq. (5) into Eq. (71) and through some calculations, we obtain

$$-q_0[p(x) - b] + 100\left[\frac{\cosh[p(x)\pi/\ell]}{\cosh(b\pi/\ell)}\right]\cos\frac{\pi x}{\ell} = 160. \tag{76}$$

Through the half-interval method we obtain $p(x)$ by the above equation with $b = \ell = 10$, $q_0 = 20$ and $u_0 = 160$ as shown in Fig. 3a with the solid line.

We are going to use the RIEM to calculate $g(x)$ when $f(x) = 10$ $q_0 + 100\cos(\pi x/\ell)/\cosh(10\pi/\ell)$ is given. Substituting Eq. (5) into Eq. (20) and through some calculations, we obtain the following regularized solution:

$$u^{\alpha}(x, p(x)) = a_0[b - p(x)] + b_0 p(x) + \left\{\frac{a_1 \sinh[(b - p(x))\pi/\ell]}{\sinh(b\pi/\ell)} + \frac{b_1 \sinh[\pi p(x)/\ell]}{\sinh(b\pi/\ell)}\right\}\cos\frac{\pi x}{\ell}, \tag{77}$$

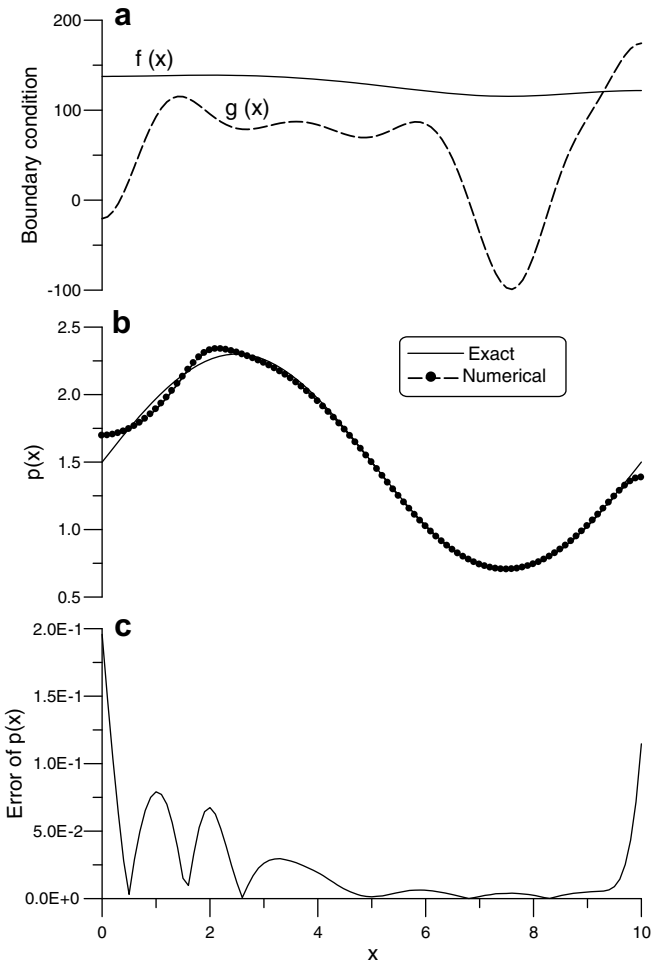

Fig. 4. For Example 2 with a sinusoidal shape we have presented the computed Dirichlet data in (a), and compared the boundary shape obtained by the numerical inverse method with the exact one in (b), and then plotted the numerical error in (c).

where

$$a_0 = q_0, \tag{78}$$

$$a_1 = \frac{100}{\cosh(b\pi/\ell)}, \tag{79}$$

$$b_0 = 0, \tag{80}$$

$$b_1 = \frac{100\pi}{\ell\alpha\sinh(b\pi/\ell)+\pi}. \tag{81}$$

For this case, we can employ $\alpha = 0$ without any difficulty because Eq. (81) is still applicable. Through the half-interval method we can acquire $p(x)$ by the above equation as shown in Fig. 3a with the dashed line, and the numerical error is zero as shown in Fig. 3b. Without exception when we use the half-interval method, the convergent criterion is fixed to be $\varepsilon_1 = 10^{-7}$.

8.2. Example 2

Substituting Eq. (18) into Eqs. (21) and (22), we can obtain

$$a_0 = \frac{1}{b}(c_1 + q_0 b), \tag{82}$$

$$a_k = \frac{c_{k+1}}{\sinh(bk\pi/\ell)}, \tag{83}$$

where $k = 1,\ldots,m$. Inserting Eq. (27) into Eqs. (55) and (56), we can get

$$b_0 = \frac{c_1}{b(1+b\alpha)}, \tag{84}$$

$$b_k = \frac{k\pi a_k \cosh(bk\pi/\ell)}{\alpha\ell\sinh(bk\pi/\ell)+k\pi}, \tag{85}$$

where $k = 1,\ldots,m$. Hence, the analytical regularized solution is given by Eq. (20) with

$$u^{\alpha}(x,y) = a_0(b-y) + b_0 y + \sum_{k=1}^{m}\left\{a_k\frac{\sinh[(b-y)k\pi/\ell]}{\sinh(bk\pi/\ell)} + b_k\frac{\sinh(k\pi y/\ell)}{\sinh(bk\pi/\ell)}\right\}\cos\frac{k\pi x}{\ell}. \tag{86}$$

Let us then consider a sinusoidal shape $p(x)$ given as follows:

$$p(x) = 1.5 + 0.8\sin\left(\frac{\pi x}{5}\right), \quad 0 \leqslant x \leqslant \ell. \tag{87}$$

We first employ the collocation method in Section 2 to find the data $f(x)$ and use the RIEM to calculate the data $g(x)$, which are plotted in Fig. 4a. In this calculation, we have fixed $\ell = 10$, $b = 3.5$, $q_0 = 20$, $u_0 = 100$, and $m = 20$. By the numerical inverse technique developed in Section 6 and the half-interval method, we can estimate $p(x)$ by using the data $f(x)$ and Eqs. (86) and (5).

The exact $p(x)$ and the computed $p(x)$ by the inverse method are compared in Fig. 4b with $\alpha = 0.001$. The dashed-dotted line shows the numerical result and the solid line displays the exact value. It can be seen that the data $p(x)$ is recovered well. Because these two curves are close, we also sketched the error in Fig. 4c, from which it can be seen that the maximum error is about 0.1957.

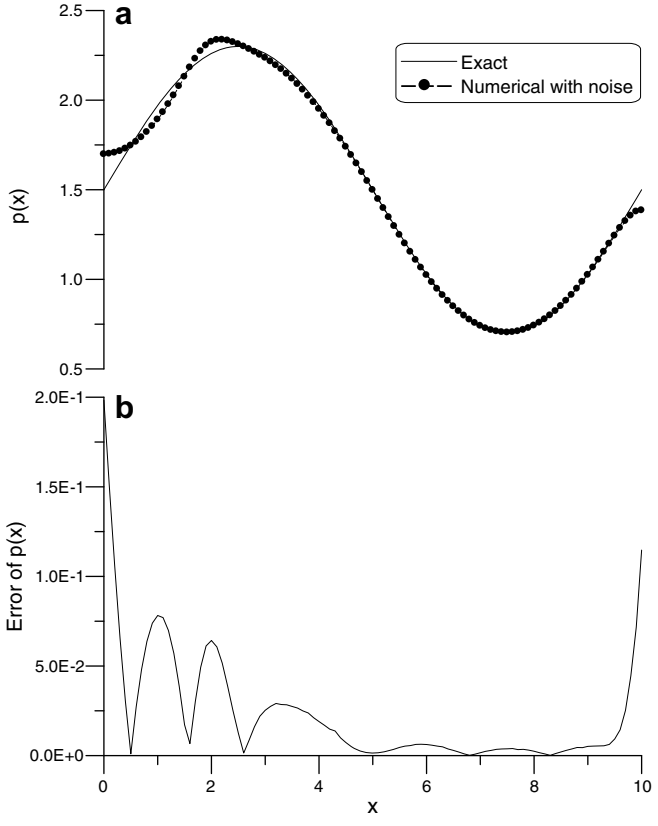

Fig. 5. For Example 2 with a sinusoidal shape we have compared the boundary shape obtained by the numerical inverse method under a noise with the exact one in (a), and then plotted the numerical error in (b).

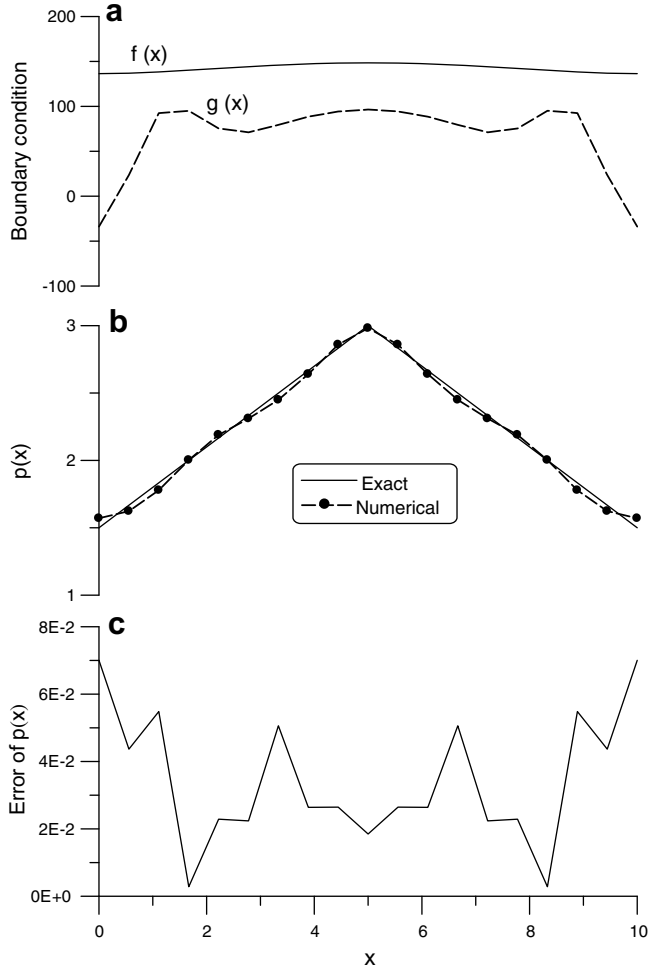

Fig. 6. For Example 3 with a triangular shape we have displayed the computed Dirichlet data in (a), and compared the boundary shape attained by the numerical inverse method with the exact one in (b), and then plotted the numerical error in (c).

In the case when the boundary measured data $f(x)$ are contaminated by random noise, we are also concerned with the stability of our algorithm. We have investigated this by adding random noise to the data $f(x)$. The numerical result with noise $\sigma = 1.0 \times 2.576$ was compared with the exact one in Fig. 5a. The factor 2.576 was chosen to represent the 99% confidence bound for the temperature measurement. It can be seen that the noise disturbs the numerical solution slightly from the one without considering noise. We also plotted the error in Fig. 5b, from which it can be seen that the maximum error is about 0.1983, which is slightly larger than the one without considering the disturbance by noise.

8.3. Example 3

Let us then consider a triangular shape $p(x)$ as follows:

$$p(x) = \begin{cases} 1.5 + 0.3x, & 0 \leqslant x \leqslant \frac{\ell}{2}, \\ 4.5 - 0.3x, & \frac{\ell}{2} \leqslant x \leqslant \ell. \end{cases} \tag{88}$$

We utilize the collocation method in Section 2 to find the data $f(x)$ and use the RIEM to calculate the data $g(x)$, which is plotted in Fig. 6a. In this calculation, we have fixed $\ell = 10$, $b = 3.5$, $q_0 = 20$, $u_0 = 100$, and $m = 20$. By the numerical inverse technique developed in Section 6 and the half-interval method, we can estimate $p(x)$ by using the data $f(x)$ and Eqs. (86) and (5). The exact $p(x)$ and the computed $p(x)$ by the inverse method are compared in Fig. 6b with $\alpha = 0.002$. The dashed-dotted line shows the numerical result and the solid line displays the exact value. It can be seen that the data $p(x)$ is recovered very well. Because these two curves are close, we also plotted the error in Fig. 6c, from which it can be seen that the maximum error is about 0.07.

The numerical result with noise $\sigma = 2.0 \times 2.576$ was compared with the exact one in Fig. 7a. It can be seen that the noise disturbs the numerical solution deviating from the exact one very small. We also sketched the error in Fig. 7b, from which it can be seen that the maximum error is about 0.07, which is slightly larger than the case without considering the disturbance by noise.

8.4. Example 4

Let us further consider a step function $p(x)$ as follows:

$$p(x) = \begin{cases} 3.0, & 0 \leqslant x \leqslant \frac{\ell}{2}, \\ 1.5, & \frac{\ell}{2} < x \leqslant \ell. \end{cases} \tag{89}$$

We use the collocation method in Section 2 to find the data $f(x)$ and use the RIEM to calculate the data $g(x)$, which is sketched in Fig. 8a. In this calculation, we have fixed $\ell = 10$, $b = 3.5$, $q_0 = 20$, $u_0 = 100$, and $m = 100$. By the numerical inverse technique developed in Section 6 and the half-interval method, we can estimate $p(x)$ by using the data $f(x)$ and Eqs. (86) and (5). The exact $p(x)$ and the computed $p(x)$ by the inverse method are compared in Fig. 8b with $\alpha = 0.0001$. The dashed-dotted line shows the numerical result and the solid line displays the exact value. We also plotted the error in Fig. 8c, from which it can be seen that the maximum error is about 1.4697.

The numerical result with noise $\sigma = 2.0 \times 2.576$ was compared with the exact one in Fig. 9a. We also plotted the error in Fig. 9b,

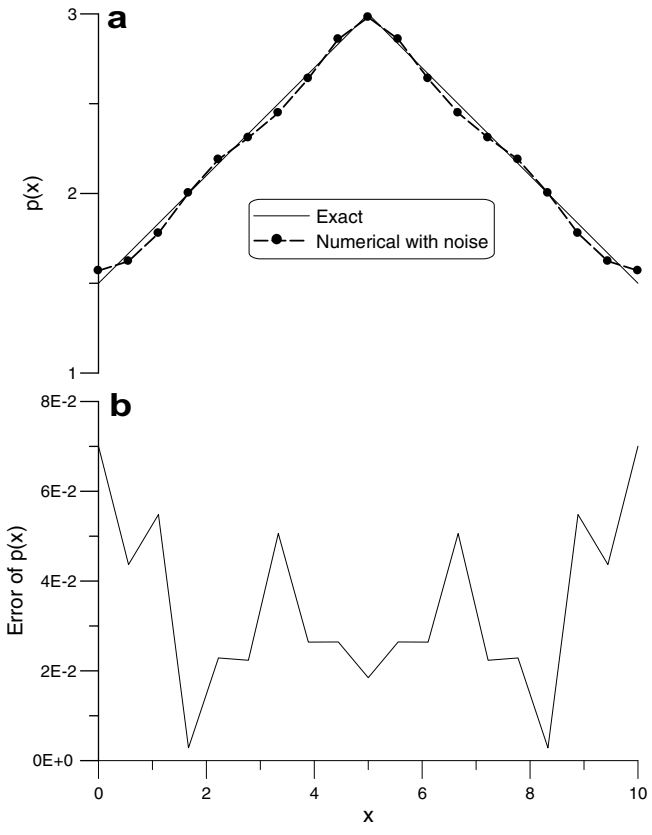

Fig. 7. For Example 3 with a triangular shape we have compared the boundary shape obtained by the numerical inverse method under a noise with the exact one in (a), and then plotted the numerical error in (b).

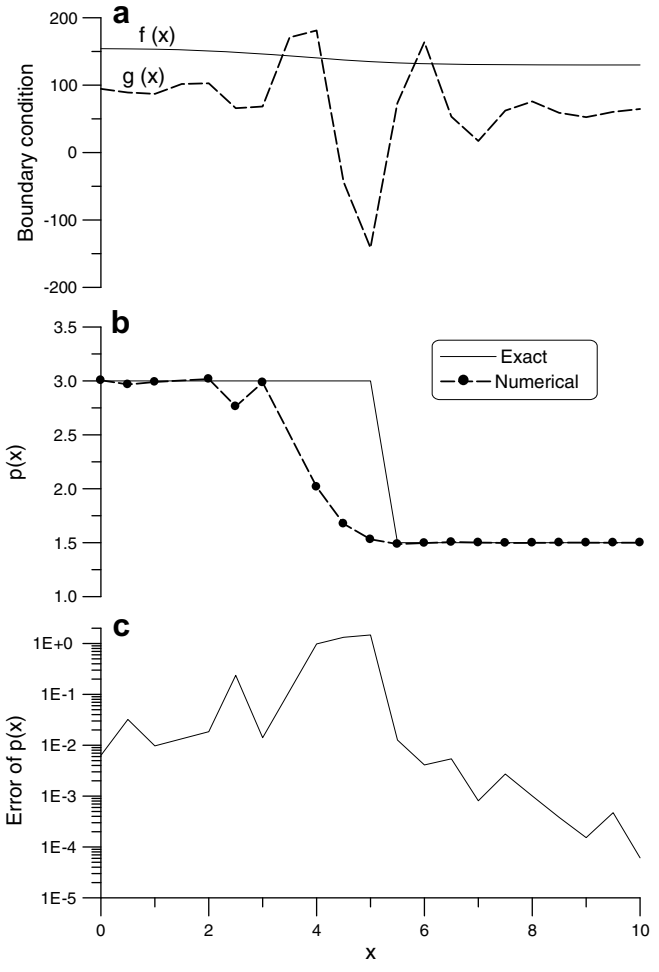

Fig. 8. For Example 4 with a step function we have showed the computed Dirichlet data in (a), and compared the boundary shape attained by the numerical inverse method with the exact one in (b), and then plotted the numerical error in (c).

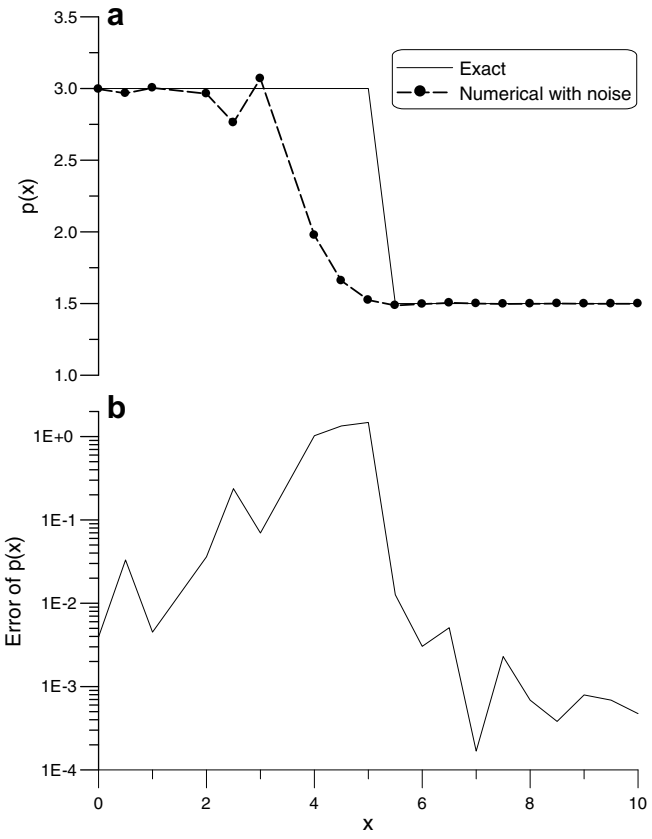

Fig. 9. For Example 4 with a step function we have compared the boundary shape obtained by the numerical inverse method under a noise with the exact one in (a), and then plotted the numerical error in (b).

from which it can be seen that the maximum error is about 1.4751, which is slightly larger than the case without considering the disturbance by noise.

Huang and Chao [5] have compared the numerical results for the above three examples calculated by the Levenberg–Marquardt and conjugate gradient algorithms. When comparing our results in Figs. 4, 6 and 8 with Figs. 2, 3, 5 and 7 in [5], it is evident that the new approach can provide a more accurate numerical result than that by the above mentioned methods. We also compare the exact result with the numerical one with noise in Figs. 5, 7 and 9 and in Figs. 4, 6 and 8 of [5]. It is obvious that our results are also better than those calculated by Huang and Chao [5].

9. Conclusions

The idea of identifying the unknown boundary configurations is modeled by an inverse Cauchy problem of the Laplace equation. First of all, we have used the collocation method to calculate the data $f(x)$ if it is not available. Then, by employing the Fourier series expansion technique and a termwise separable property of kernel function, an analytical solution for approximating the inverse problem is presented. The uniform convergence and error estimate of the regularized solution are provided and a boundary geometry $p(x)$ is solved by using the half-interval method. Several numerical examples have shown that the current approach can identify the unknown irregular boundary configurations very well, and excellent numerical results are obtained even under a large noise disturbance on the measured data.

References

[1] O.M. Alifanov, Solution of an inverse problem of heat conduction by iteration methods, J. Eng. Phys. 26 (1972) 471–476.
[2] C.H. Huang, M.N. Ozisik, Inverse problem of determining unknown wall heat flux in laminar flow through a parallel plate duct, Numer. Heat Transfer A 21 (1992) 55–70.
[3] C.H. Huang, M.N. Ozisik, B. Sawaf, Conjugate gradient method for determining unknown contact conductance during metal casting, Int. J. Heat Mass Transfer 35 (1992) 1779–1786.
[4] C.H. Huang, J.Y. Yan, An inverse problem in simultaneously measuring temperature dependent thermal conductivity and heat capacity, Int. J. Heat Mass Transfer 38 (1995) 3433–3441.
[5] C.H. Huang, B.H. Chao, An inverse geometry problem in identifying irregular boundary configurations, Int. J. Heat Mass Transfer 40 (1997) 2045–2053.
[6] C.H. Huang, T.Y. Hsiung, An inverse design problem of estimating optimal shape of cooling passages in turbine blades, Int. J. Heat Mass Transfer 42 (1999) 4307–4319.
[7] C.H. Huang, H.M. Chen, An inverse geometry problem of identifying growth of boundary shapes in a multiple region domain, Numer. Heat Transfer A 35 (1999) 435–450.
[8] C.H. Huang, C.C. Shih, Identify the interfacial configurations in a multiple region domain problem, AIAA J. Thermophys. Heat Transfer 19 (2005) 533–541.
[9] C.H. Huang, C.C. Shih, A shape identification problem in estimating simultaneously two interfacial configurations in a multiple region domain, Appl. Therm. Eng. 26 (2006) 77–88.
[10] C.H. Cheng, M.H. Chang, A simplified conjugate-gradient method for shape identification based on thermal data, Numer. Heat Transfer B 43 (2003) 489–507.
[11] C.H. Huang, C.C. Chiang, Shape identification problem in estimating geometry of multiple cavities, AIAA J. Thermophys. Heat Transfer 12 (1998) 270–277.
[12] C.K. Hsieh, K.C. Su, A methodology of predicting cavity geometry based on the scanned surface temperature data-prescribed surface temperature at the cavity side, J. Heat Transfer 102 (1980) 324–329.
[13] S. Das, A. Mitra, An algorithm for the solution of inverse Laplace problems and its application in flaw identification in materials, J. Comput. Phys. 99 (1992) 99–105.
[14] A.J. Kassab, J. Pollard, A cubic spline anchored grid pattern algorithm for high resolution detection of subsurface cavities by the IR-CAT method, Numer. Heat Transfer B 26 (1994) 63–78.
[15] C.-S. Liu, Elastic torsion bar with arbitrary cross-section using the Fredholm integral equations, CMC: Comput. Mater. Continua 5 (2007) 31–42.
[16] C.-S. Liu, A meshless regularized integral equation method for Laplace equation in arbitrary interior or exterior plane domains, CMES: Comput. Model. Eng. Sci. 19 (2007) 99–109.
[17] C.-S. Liu, A MRIEM for solving the Laplace equation in the doubly-connected domain, CMES: Comput. Model. Eng. Sci. 19 (2007) 145–161.
[18] M.M. Lavrentiev, Some Improperly Posed Problems of Mathematical Physics, Springer, New York, 1967.
[19] G. Marsaglia, M.D. MacLaren, T.A. Bray, A fast procedure for generating normal random variables, Commun. ACM 7 (1964) 4–10.